DR. JENNIFER KOLLMER (Orcid ID : 0000-0002-6254-9192)

Article type : Original Article

Quantitative magnetic resonance neurographic characterization of peripheral nerve involvement in manifest and pre-ataxic spinocerebellar ataxia type 3

Original research article

Jennifer Kollmer, MD,[1] Markus Weiler, MD,[2] Georges Sam, PhD,[2] Jennifer Faber, MD,[3,4] John M. Hayes, BA,[5] Sabine Heiland, PhD,[1,6] Martin Bendszus, MD,[1] Wolfgang Wick, MD,[2,7] and Heike Jacobi, MD[2]

[1] Department of Neuroradiology, Heidelberg University Hospital, Heidelberg, Germany

[2] Department of Neurology, Heidelberg University Hospital, Heidelberg, Germany

[3] Department of Neurology, Bonn University Hospital, Bonn, Germany

[4] German Center for Neurodegenerative Diseases, Bonn, Germany

[5] Department of Neurology, University of Michigan, Ann Arbor, USA

[6] Division of Experimental Radiology, Department of Neuroradiology, Heidelberg University Hospital, Heidelberg, Germany

[7] Clinical Cooperation Unit Neurooncology, German Cancer Research Center/DKTK, Heidelberg. Germany

Corresponding Authors:

Jennifer Kollmer, MD

Department of Neuroradiology

Heidelberg University Hospital

This is the author manuscript accepted for publication and has undergone full peer review but has not been through the copyediting, typesetting, pagination and proofreading process, which may lead to differences between this version and the Version of Record. Please cite this article as doi: 10.1111/ENE.15305

Im Neuenheimer Feld 400
D-69120 Heidelberg
Germany
Phone: +49 6221 567566
Fax: +49 6221 564673
Email: jennifer.kollmer@med.uni-heidelberg.de

Heike Jacobi, MD
Department of Neurology
Heidelberg University Hospital
Im Neuenheimer Feld 400
D-69120 Heidelberg
Germany
Phone: +49 6221 5636328
Fax: +49 6221 566812
Email: heike.jacobi@med.uni-heidelberg.de

Running title

MR neurography in SCA3

Key Words

Electrophysiology, magnetic resonance neurography (MRN), polyneuropathy, quantitative imaging markers, spinocerebellar ataxia.

Funding

The study was supported in part by the Medical Faculty of the University of Heidelberg (Olympia Morata stipend grant to J.K. & H.J.), and the German Research Foundation (SFB 1118 to S.H., SFB 1158 to M.B.).

Disclosure of conflict of interest

J. Kollmer received a research grant, personal fees, lecture honoraria and financial support for conference attendance from Alnylam Pharmaceuticals, the Olympia Morata stipend grant from the Medical Faculty of the University of Heidelberg, lecture honoraria and financial support for conference attendance from Pfizer, and advises for Akcea Therapeutics.

M. Weiler advises for Akcea Therapeutics, Alnylam Pharmaceuticals, Biogen, Pfizer, Roche, and Sobi, received lecture honoraria from Akcea Therapeutics, Alnylam Pharmaceuticals, Biogen, and Roche, and received financial support for conference attendance from Biogen, and Pfizer.

G. Sam reports no disclosures relevant to this work.

J. Faber received funding from the National Ataxia Foundation (NAF) and is a fellow of the Hertie Academy for Clinical Neuroscience.

J.M. Hayes reports no disclosures relevant to this work.

S. Heiland received research grants from the German Research Foundation (SFB 1118) and from the Dietmar Hopp Foundation.

M. Bendszus reports personal fees from Boehringer Ingelheim, grants and personal fees from Novartis, and Guerbet, grants from Siemens, the Hopp Foundation, the German Research Foundation (SFB 1158), the European Union, and Stryker, personal fees from Merck, Bayer, Teva, BBraun, Vascular Dynamics, Grifols, and Neuroscios.

W. Wick reports no disclosures relevant to this work.

H. Jacobi received the Olympia Morata stipend grant from the Medical Faculty of the University of Heidelberg.

Word count 5,642 (3,500 main body of the manuscript)

Acknowledgements

The authors thank Gustav Neitz, Department of Neuroradiology, Heidelberg University Hospital, for scheduling patient appointments.

Abstract

Background:

Knowledge about the exact underlying pathophysiologic changes involved in the genesis and progression of spinocerebellar ataxia (SCA3) is limited. We characterized and quantified lower extremity peripheral nerve lesions in clinically, genetically, and electrophysiologically

classified ataxic and pre-ataxic SCA3 mutation carriers by magnetic resonance neurography (MRN).

Methods:

18 SCA3 mutation carriers and 20 age-/sex-matched healthy controls were prospectively enrolled. All SCA3 mutation carriers underwent detailed neurologic and electrophysiologic examinations. 3T MRN covered the lumbosacral plexus and proximal thigh to the tibiotalar joint by using T2-weighted inversion-recovery sequences, dual-echo relaxometry sequences with spectral fat saturation, and two gradient-echo sequences with and without an off-resonance saturation rapid frequency pulse. Detailed quantification of nerve lesions by morphometric and microstructural MRN markers, including T2-relaxometry and magnetization transfer contrast imaging, was conducted in all study participants.

Results:

MRN detected peripheral nerve damage in ataxic and pre-ataxic SCA3. The quantitative markers, proton spin density (ρ), T2-relaxation time, magnetization transfer ratio (MTR), and cross-sectional area, were decreased in SCA3, indicating chronic axonopathy. MTR and ρ identified early, subclinical nerve damage in pre-ataxic SCA3 and in SCA3 mutation carriers without polyneuropathy, and were superior in differentiating between all subgroups. Additionally, microstructural markers correlated well with clinical symptom scores and electrophysiologic results.

Conclusions:

Our data provide a comprehensive characterization of peripheral nerve damage in SCA3 and assist in understanding the mechanisms of the multisystemic disease evolution. Evidence of peripheral nerve involvement prior to the onset of clinically overt ataxia might have important implications for designing early intervention studies.

Introduction

Spinocerebellar ataxias (SCA) are heterogeneous autosomal dominant inherited ataxic disorders leading to progressive disability and premature death. The most common subtype worldwide is spinocerebellar ataxia type 3 (SCA3).(1)

SCA3 affects not only the cerebellum but several regions of the nervous system such as basal ganglia, brainstem, thalamus, spinal cord, dorsal root ganglia, and peripheral nerves.(2) As SCA3 is caused by CAG trinucleotide repeat expansions in the *ATXN3* gene with full penetrance, pre-ataxic mutation carriers provide the unique opportunity to study early pathophysiologic changes. Age at onset of SCA3 is mainly in the 3rd or 4th decade, but is highly variable, partly depending on the repeat length of the expanded allele.(3) Clinically, progressive ataxia is the most prominent feature,(4) but the majority of SCA3 patients show clinical symptoms and electrophysiologic evidence of an additional peripheral neuropathy with sensory disturbances, areflexia, weakness, and muscle wasting.(5)·(6)

In previous studies, magnetic resonance neurography (MRN) detected and localized peripheral nerve lesions *in vivo* at early, even presymptomatic disease stages in different diffuse neuropathies.(7-10) With this explorative study, we aim to characterize lower extremity peripheral nerve lesions by MRN in genetically, clinically, and electrophysiologically classified pre-ataxic and ataxic SCA3 mutation carriers in comparison with healthy controls. To quantify peripheral nerve damage on a macroscopic and microstructural level, we performed T2-relaxometry, magnetization transfer contrast (MTC) imaging, and morphometric quantification.

Methods

Study design, neurologic and electrophysiologic assessments

This prospective case-control study was approved by the institutional ethics board (University of Heidelberg; S-398/2012), and all participants gave written informed consent.

18 SCA3 mutation carriers (9 males, 9 females, mean age 41.2±2.9 years, range 22–64 years) and 20 age- and sex-matched healthy volunteers (10 males, 10 females, 41.4±2.9 years, range 21–64 years) were enrolled from May 2017 to August 2020. Exclusion criteria were ruled out based on patients´ past medical history and medical records, comprising age <18 years, pregnancy, concomitant causes of polyneuropathy (PNP) (diabetes mellitus, hypothyroidism, Vitamin B12 deficiency), malignant or infectious diseases, neurologic disorders other than SCA3, and contraindications for MRI. Known exposure to environmental or occupational exogenous noxae, previous treatment with chemotherapies, cytostatics, or other potentially neurotoxic drugs were further exclusion criteria.

Severity of ataxia was assessed using the Scale for the Assessment and Rating of Ataxia (SARA),(11) while neurologic signs other than ataxia (e.g., impaired vibration sense, tendon reflexes) were documented with the Inventory of Non-Ataxia Signs (INAS).(12) Pallesthesia was graded as none (8/8), mild (5-7/8), moderate (2-5/8), or severe (<2/8). Mutation carriers were classified as either pre-ataxic or ataxic with manifest ataxia being defined by a SARA score of ≥3.(11)

The presence of PNP in our cohort was solely defined based on electroneurographic results, as clinical assessments may be influenced by potentially overlapping clinical symptoms originating from spinal cord or brain pathologies. For this purpose, motor nerve conduction studies assessed distal motor latencies (DML), compound muscle action potentials (CMAP), and nerve conduction velocities (NCV) of the right peroneal and left tibial nerves. Sensory nerve action potentials (SNAP) and NCVs were measured for the right and left sural nerves (G.S.,M.W.; Natus, Keypoint G4, Version 2.4). Skin temperature was controlled at a minimum of 32°C. PNP was diagnosed when either CMAP or SNAP amplitudes were pathologic in at least two different leg nerves, according to in-house validated reference parameters, after exclusion of focal entrapment neuropathies and innervation variants.

For pre-ataxic mutation carriers, we calculated the predicted age of ataxia onset based on the CAG repeat length.(13)

MRN protocol

All participants underwent the following high-resolution MRN protocol in a 3.0 Tesla MR-scanner (Magnetom PRISMA, Siemens-Healthineers, Erlangen, Germany):

(1) 3D T2w inversion-recovery SPACE (**S**ampling **P**erfection with **A**pplication-optimized **C**ontrasts using different flip angle **E**volution) sequence for imaging of the lumbar plexus and spinal nerves with 50 axial reformations/patient: repetition-time (TR)/echo-time (TE)/inversion-time (TI) 3000/205/210ms, field-of-view (FoV) 305x305mm^2, matrix-size 320x320x104, slice thickness 1.0mm, no gap, voxel-size 1.0x1.0x1.0mm^3, acquisition time 8:35 min.

(2) Axial dual-echo turbo-spin-echo 2D-sequence with spectral fat saturation for T2-relaxometry with four continuous slabs at the left leg: Slab1: proximal thigh to mid-thigh; slab2: mid-thigh to distal thigh with alignment of the distal edge of this imaging-slab on the tibiofemoral joint space; slab3: lower leg with alignment of its proximal edge with the tibiofemoral joint space; slab4: ankle level with alignment of the distal edge on the tibiotalar joint space. One additional slab was acquired at the right mid to distal thigh. Sequence parameters were: TR 5860ms, TE_1 14ms, TE_2 86ms, FoV 170x170mm^2, matrix-size 512x512, slice thickness 3.5mm, interslice gap 0.35mm, voxel-size 0.3x0.3x3.5mm^3, flip angle 180°, 35 slices, acquisition time per slab 8:25min.

(3) Two axial three-dimensional, gradient-echo sequences with and without an off-resonance saturation pulse (Gaussian envelop, duration 9984µs, frequency offset 1200Hz) were carried out at the exact same slice position at the right mid- to distal thigh: TR 50ms, TE 4.92ms, FoV 160x160mm², matrix-size 256x256, band-width 370 Hz/Px, slice thickness 3.5mm, voxel-size 0.6x0.6x3.5mm³, flip angle 7°, 16 slices, acquisition time per sequence 3:48min.

Net acquisition time including survey scans was 61:35 minutes. Patient and coil repositioning required additional 20-30minutes. An 18-channel body-array flex-coil (Siemens-Healthineers) was used for imaging of the lumbar plexus (sequence (1)), and a 15-channel transmit-receive extremity-coil (INVIVO, Gainesville, FL, USA) for imaging of the left and right leg (sequences (2) and (3)).

Image post-processing and analyses

All images were analyzed in ImageJ (version 1.52v; National Institutes of Health, Bethesda, MD, USA). Tibial fascicles of the left sciatic nerve and their distal continuation as tibial nerve with coverage from the proximal thigh down to the distal ankle were segmented on 140 axial slices/participant generated by sequence (2) by one neuroradiologist (J.K.) blinded to clinical data. To exclude significant side differences, the tibial nerve was additionally segmented on 35 axial slices at the right mid- to distal thigh, a region where previous studies predominantly identified nerve lesions in different neuropathies.(7, 14-16)

For the same reason, MTC imaging was performed at the distal thigh. To avoid any potential inaccuracies in identifying tibial or peroneal fascicles due to the lower resolution of MTC sequences, we decided to segment the whole sciatic nerve on ten consecutive slices at the center of sequence (3), approximately 1 cm proximal of the nerve bifurcation (J.K.).

Signal quantification

The apparent T2 relaxation time ($T2_{app}$, equation 1) and proton spin density (ρ, equation 2) were calculated by using relaxometry data (sequence (2)) with TE_1 set at 14 ms and TE_2 set at 86 ms.(17)

$$T2app = \frac{\mathrm{TE}_2 - TE_1}{\ln\left(\frac{SI(TE1)}{SI(TE2)}\right)}$$

$$\rho = \frac{SI(TE_1)}{\exp\left(\frac{TE_1}{T2_{app}}\right)}$$

Mean values of nerve ρ and $T2_{app}$ were calculated per slice position for each participant. Subsequently, we compared averaged mean ρ and $T2_{app}$ values of the tibial nerve at the thigh (imaging slabs 1 and 2) to respective mean values of the lower leg (imaging slabs 3 and 4) to test for potential location-dependent differences along the proximal-to-distal course of the tibial nerve. Further analyses were conducted to test for differences between subgroups (SCA3, SCA3 with PNP (SCA3 PNP+), SCA3 without PNP (SCA3 PNP-), pre-ataxic mutation carriers, controls).

Magnetization transfer contrast imaging

The magnetization transfer ratio (MTR) was calculated separately for each participant, and each evaluated axial imaging slice according to the following equation, in which S_0 is the signal without and S_1 with off-resonance saturation:

$$\mathrm{MTR} = 100\ \mathrm{x}\frac{(\mathrm{S}_0 - \mathrm{S}_1)}{\mathrm{S}_0}$$

MTR values were subsequently extracted from each slice position and averaged over all slice positions for each participant. Computed sciatic nerve MTR mean values were then compared between the different groups.

Morphometric quantification

Tibial nerve caliber was measured as cross-sectional area (CSA) on each axial slice for morphometric quantification. Bilateral proximal spinal nerves L5 and S1 were additionally segmented on axial reformations of sequence (1). The lumbosacral plexus was segmented at the level of the sciatic notch on both sides.

Statistical analyses

Statistical data analyses were performed in GraphPad Prism 9.0.2 (J.K.,J.M.H.). Differences between SCA3 and controls, pre-ataxic mutation carriers and controls, the left and right distal thigh, and the thigh and the lower leg were evaluated with the Mann-Whitney test. Subgroup analyses between SCA3 PNP+, SCA3 PNP-, and controls were performed by using a one-way ANOVA for *a priori* assumptions. Subsequent *post hoc* analyses were corrected for multiple comparisons by using the Tukey-Kramer test. Pearson's correlation coefficients were calculated for correlation analyses between MRN parameters and demographic (age, sex, height, weight, body mass index (BMI)), clinical (duration of symptoms, SARA, INAS, pallesthesia, CAG expanded and normal allele) and electrophysiologic (tibial and peroneal NCV, DML, CMAP, and sural nerve NCV and SNAP) results. Statistical tests were two-tailed and an alpha level of significance was defined at $p<0.05$. All results are documented as mean values±SEM.

All data used to conduct this study are documented in the "Methods" section. Additional anonymized datasets will be shared by the request from any qualified investigator.

Results

Clinical and electrophysiologic data

Seven of the 18 SCA3 mutation carriers were classified as pre-ataxic defined by a SARA score of <3. Six of the 11 ataxic and none of the pre-ataxic mutation carriers fulfilled the electrophysiologic criteria for PNP. There were no differences with respect to the CAG repeat

length of the mutated allele, but SCA3 PNP+ showed an older age, higher SARA scores, and higher INAS counts (Table 1). Mean predicted age of ataxia onset in pre-ataxic mutation carriers calculated on the basis of CAG repeat length was –4.89 years. Detailed demographic and clinical characteristics are given in Table 1.

MRN data

Proton spin density (ρ)

Tibial nerve ρ was markedly decreased in SCA3 (390.8±14.5a.u.) versus controls (472.8±10.4a.u.; p<0.0001; Figure 1A) at the thigh and at the lower leg (SCA3: 384.0±14.6a.u. versus controls 449.4±13.9a.u.; p=0.0013). When subdividing the SCA3 group into SCA3 PNP+ and SCA3 PNP-, group differences were identified at the thigh (p<0.0001, F=11.98), and at the lower leg (p=0.0013; F=7.440). Subsequent *post hoc* analyses revealed that nerve ρ at the thigh was lower in SCA3 PNP+ (362.7±16.2a.u.; p=0.0002) and in SCA3 PNP- (403.1±19.2a.u.; p=0.0018) versus controls, but differences between the two SCA3 groups did not exist (p=0.31; Figure 1A). At the lower leg, ρ was only lower in SCA3 PNP+ (339.54±20.2a.u.; p=0.0013) versus controls. Furthermore, a decrease in tibial nerve ρ was already found in pre-ataxic SCA3 (thigh: 392.7±26.7a.u.; lower leg: 397.5±25.2a.u.) versus controls (thigh: p=0.0016; Figure 1A; lower leg: p=0.0442). A proximal-to-distal gradient or a difference between the left and right thigh was absent in SCA3 and controls (p>0.05).

An inverse correlation was identified between tibial nerve ρ at the thigh and the SARA (r=-0.45, p=0.0093) and INAS score (r=-0.40, p=0.0219). Consistent correlations between tibial nerve ρ at thigh or lower leg level and any of the remaining demographic, clinical or electrophysiologic parameters did not exist.

Apparent T_2-relaxation time ($T2_{app}$)

Tibial nerve $T2_{app}$ at thigh level was lower in SCA3 (63.9±0.9ms) than in controls (67.1±0.8ms; p=0.0137; Figure 1B), and was also decreased at the lower leg in SCA3 (61.1±1.1ms) versus controls (64.9±1.1ms; p=0.0136). ANOVA indicated subgroup differences at the thigh (p=0.0082; F=5.180), but not at the lower leg (p=0.06; F=2.943). In detail, $T2_{app}$ at the thigh was lower in SCA3 PNP+ (61.9±1.3ms) versus controls (p=0.0093), while no differences existed between SCA3 PNP- (64.7±1.1ms) and controls (p=0.14) or between SCA3 PNP+ and SCA3 PNP- (p=0.28; Figure 1B). Differences in $T2_{app}$ between pre-ataxic SCA3 (thigh: 64.6±1.5ms; lower leg: 61.9±1.3ms) and controls were not observed (thigh: p=0.16; Figure 1B;

lower leg: p=0.15). A slight proximal-to-distal gradient in $T2_{app}$ was found in SCA3 (p=0.0268) and controls (p=0.0428). Side differences did not exist in SCA3 or controls (p>0.05).

Correlation analyses revealed an inverse correlation between tibial nerve $T2_{app}$ at thigh level and the INAS (r=-047, p=0.0055), and positive correlations with peroneal CMAP (r=0.52, p=0.0017), tibial NCV (r=0.38, p=0.0310), and sural SNAPs (r=0.53, p=0.0029). At the lower leg, tibial nerve $T2_{app}$ correlated with peroneal CMAPs (r=0.37, p=0.0317) and sural SNAPs (r=0.36, p=0.0452).

Magnetization transfer ratio (MTR)

Sciatic nerve MTR was clearly reduced in SCA3 (28.1±0.5%) versus controls (33.0±0.5%, p<0.0001; Figure 1C). ANOVA revealed marked differences between SCA3 PNP+, SCA3 PNP-, and controls (p<0.0001; F=32.78). In detail, MTR values were lower in SCA3 PNP+ (25.9±0.9%, p<0.0001) and SCA3 PNP- (29.2±0.4%, p<0.0001) versus controls, and were also lower in SCA3 PNP+ versus SCA3 PNP- (p=0.0094; Figure 1C, Figure 3). Additional analyses showed that the MTR was already decreased in pre-ataxic SCA3 (29.7±0.5%) versus controls (p=0.0006; Figure 1C).

Sciatic nerve MTR showed an inverse correlation with age (r=-0.71, p=0.0028), but not with other demographic parameters. Inverse correlations were found between MTR and disease duration (r=-0.62, p=0.0097), SARA (r=-0.57, p=0.0225), INAS (r=-0.60, p=0.0146), and pallesthesia (r=-0.5103, p=0.0434). MTR also correlated well with peroneal (r=0.65, p=0.0063) and tibial NCV (r=0.73, p=0.0068) as well with peroneal (r=0.61, p=0.0254) and tibial CMAPs (r=0.72, p=0.0016), and sural SNAPs (right: r=0.71, p=0.0031, left: r=0.69, p=0.0067).

Cross sectional area

CSA of the tibial nerve was markedly lower in SCA3 (12.1±0.3 mm²) versus controls (14.2±0.3 mm²; p<0.0001; Figure 1D) at the thigh and at the lower leg (SCA3: 6.3±0.3 mm² versus controls: 7.2±0.2 mm²; p=0.0181). Differences between subgroups were detected at the thigh (p<0.0001; F=11.58), but not at the lower leg (p=0.06; F=3.020). At the thigh, CSA was decreased in SCA3 PNP+ (12.5±1.0 mm²; p=0.0361) and SCA3 PNP- (11.9±0.3 mm²; p<0.0001) versus controls, while no CSA differences were detected between the two SCA3 subgroups (p=0.63; Figure 1D). Tibial nerve CSA was also different between controls and pre-ataxic SCA3 (12.1±0.3 mm²; p=0.0003; Figure 1D) at the thigh, but not at the lower leg (p=0.07). Consistent with the physiologic decrease in nerve caliber, tibial nerve CSA was

markedly higher at the thigh than at the lower leg in SCA3 and controls ($p<0.0001$, respectively). Side differences between right and left tibial nerve CSAs were not observed in SCA3 or controls ($p>0.05$).

Tibial nerve CSA at thigh level correlated positively with patient weight ($r=0.43$, $p=0.0164$) and BMI ($r=0.36$, $p=0.0447$). No further consistent correlations were found between tibial nerve CSA and any of the remaining evaluated parameters.

Analyses of proximal spinal nerves and the lumbosacral plexus revealed no differences in CSA between SCA3 (L5: 3.9±0.2 mm²; S1: 4.0±0.2 mm²; plexus: 7.4±0.4 mm²) and controls (L5: 3.8±0.3 mm², $p=0.53$; S1: 3.7±0.2 mm², $p=0.21$; plexus: 8.0±0.5 mm², $p=0.33$). Therefore, we performed no further analyses in the SCA3 subgroups.

Discussion

SCA3 is a multisystemic disease that affects different anatomic regions within the CNS and PNS, frequently leading to central neurologic symptoms and signs of peripheral neuropathy.(2,4,6) Knowledge about the exact mechanisms preceding disease onset and leading to disease progression is limited.

Here, we report on the first comprehensive characterization and quantification of peripheral nerve involvement in pre-ataxic and ataxic SCA3 mutation carriers by applying quantitative MRN. Our results show that (i) all evaluated microstructural and morphometric quantitative MRN parameters are markedly decreased in SCA3 compared to controls, (ii) nerve impairment is also detectable in pre-ataxic mutation carriers and in SCA3 patients without PNP, and (iii) ρ and MTR are the most suitable MRN markers to allow an early diagnosis and differentiation between subgroups while correlating well with disease severity.

ρ and $T2_{app}$ are known to be microstructural markers of nerve tissue integrity *in vivo*, depending on the macromolecular composition of nerve tissue.(17-19) Both markers were recently established for the quantification of nerve lesions in various PNS diseases by our group, and have become increasingly important on the path to developing imaging biomarkers.(7,9,15,20,21) Recent studies consistently concluded that typical, distal-symmetric PNPs of different etiologies, are characterized by an early increase of ρ, followed by an additional increase in $T2_{app}$ in symptomatic PNP.(7,9,15,22) In contrast, nerve injury in 5q-linked SMA as an example for a neurodegenerative motor neuron disease, was characterized by

a decrease in ρ (opposite to results in PNPs) and an increase in $T2_{app}$ (similar to results in PNPs),(8) while peripheral nerve involvement in multiple sclerosis (MS), an example of a demyelinating disease, showed an increase in ρ (similar to results in PNPs) and a decrease in $T2_{app}$ (opposite to results in PNPs).(21)

Our finding of a combined decrease in ρ and $T2_{app}$ in SCA3 is unique among the multitude of diffuse neuropathies investigated by MRN so far, representing a different pathomechanism of peripheral neuropathy in SCA3. Electrophysiologically, peripheral nerve involvement in SCA3 presents as a pure axonal neuropathy with sensory or sensorimotor symptoms, partially accompanied by fasciculations.(23,24) The axonal damage in SCA3 is a likely explanation for the observed decrease of ρ in SCA3. It has been similarly described in SMA where the decay of lower motor neurons with subsequent axonal loss is the predominant pathomorphologic hallmark.(8) However, the reactive increase in $T2_{app}$ detected in SMA, hypothetically induced by nerve edema, was absent in our SCA3 cohort. The decrease of nerve ρ in our study points against demyelination as a relevant factor in the development of peripheral neuropathy in SCA3. Areas of increased ρ in the brain of deceased MS patients were previously histopathologically correlated with areas of demyelination,(25) and in a recent MRN study conducted in MS patients, peripheral nerve lesions were associated with an increase in ρ, leading to the hypothesis of a peripheral co-demyelination.(21) In SCA3, additional demyelinating components are uncommon and would rather point towards SCA mimicking immunologic or neurometabolic diseases.(24) Instead, the additional decrease in tibial nerve CSA indicates neuronal atrophy, further supporting the hypothesis of a chronic degenerative process in SCA3 characterized by predominant axonal loss.

MTC imaging provides additional information on the concentration of protons bound to macromolecules, that cannot be directly measured by conventional MRI sequences, and their interaction with free water molecules.(26-29) The first study applying MTC imaging in neuropathic patients was conducted in Charcot-Marie-Tooth disease type 1A (CMT1A), where MTR correlated well with the grade of disability.(30) These promising results were recently confirmed in hereditary transthyretin (ATTRv) amyloidosis, where MTR correlated well with clinical PNP symptom scores and electrophysiologic results, and detected early nerve damage in clinically and electrophysiologically completely asymptomatic carriers of the variant *transthyretin* gene.(31) In initial studies, it was assumed that a MTR decrease indicates the

degree of demyelination, but other studies favored a reduced axonal density as the origin for a reduced MTR.(26) The latter hypothesis was supported by the finding of decreased nerve MTR values in SMA, where axonal loss accounts for the predominant pathomorphologic fingerprint,(32) and is likely the underlying reason for the MTR decrease observed in our SCA3 cohort. Moreover, sciatic nerve MTR was the sole MRN marker that differentiated SCA3 PNP- not only from healthy controls (similar to ρ, $T2_{app}$, and CSA), but also from SCA3 PNP+. Even though MTR decreases in pathophysiologically completely different disease entities like CMT1A, ATTRv amyloidosis, SMA, and SCA3, making it an unspecific MRN marker, it might be the most promising and sensitive biomarker to differentiate between SCA3 subgroups, and to detect early nerve injury in pre-ataxic and SCA3 PNP- mutation carriers.

In our study cohort, 6 of the 11 ataxic and none of the pre-ataxic SCA3 mutation carriers fulfilled the electrophysiologic criteria for PNP. Conversely, quantitative MRN markers, especially MTR, showed a gradual decrease from controls over SCA3 PNP- to SCA3 PNP+, and from controls to pre-ataxic SCA3. Particularly, our finding of a significant decrease in ρ, MTR, and CSA in pre-ataxic SCA3 mutation carriers indicate that – even without electrophysiologic signs of PNP – mild peripheral nerve involvement is already present in the pre-ataxic stage, but remains clinically inapparent until a certain threshold is exceeded.

Quantitative MRN markers correlated well with the SARA, INAS, and electrophysiologic results, but are more objective and observer independent compared to clinical rating scales, making quantitative MRN markers promising supportive tools for monitoring disease progression in the future.

The cross-sectional design of our study does not allow an interpretation regarding the temporal progression of structural nerve damage. Future longitudinal studies assessing MRN in correlation with clinical and electrophysiologic disease progression would be desirable, and are part of ongoing follow-up examinations. This approach will prove if quantitative MRN parameters can be used as progression biomarkers in clinical trials. Here, the acquisition time for the MRN protocol may be markedly reduced by limiting the recording of quantitative data to one leg and one anatomic location. Future studies should also test the potential of high-resolution nerve ultrasound to detect peripheral nerve lesions in SCA3, as ultrasound might be more broadly available than MRN. Another limitation is the small number of participants.

However, we concentrated on SCA3, the most common SCA subtype, for our exploratory study as recruitment of a sufficiently large number of mutation carriers of all other genotypes was not feasible at our center.

Our study results provide comprehensive data on the *in vivo* characterization of peripheral nerve damage in SCA3 that help to understand the mechanisms behind the multisystemic disease evolution. While all analyzed MRN markers differentiated well between healthy controls and SCA3 mutation carriers, ρ and MTR are most suited to differentiate between SCA3 subgroups, and to identify pre-ataxic and SCA3 PNP- mutation carriers. The identification of peripheral nerve involvement in pre-ataxic SCA3 mutation carriers by MRN as an early sign of disease manifestation might have important implications for the planning of future preventive clinical trials as therapeutic strategies might target SCA3 mutation carriers prior to the onset of clinically manifest ataxia and before irreversible brain damage occurs.

References

1. Ruano L, Melo C, Silva MC, Coutinho P. The global epidemiology of hereditary ataxia and spastic paraplegia: a systematic review of prevalence studies. Neuroepidemiology. 2014;42(3):174-83.
2. Koeppen AH. The Neuropathology of Spinocerebellar Ataxia Type 3/Machado-Joseph Disease. In: Nobrega C, Pereira de Almeida, L., editor. Polyglutamine Disorders Advances in Experimental Medicine and Biology. 1049: Springer; 2018.
3. Klockgether T, Mariotti C, Paulson HL. Spinocerebellar ataxia. Nat Rev Dis Primers. 2019;5(1):24.
4. Mendonca N, Franca MC, Jr., Goncalves AF, Januario C. Clinical Features of Machado-Joseph Disease. Adv Exp Med Biol. 2018;1049:255-73.
5. van de Warrenburg BP, Notermans NC, Schelhaas HJ, van Alfen N, Sinke RJ, Knoers NV, et al. Peripheral nerve involvement in spinocerebellar ataxias. Arch Neurol. 2004;61(2):257-61.
6. Schmitz-Hubsch T, Coudert M, Bauer P, Giunti P, Globas C, Baliko L, et al. Spinocerebellar ataxia types 1, 2, 3, and 6: disease severity and nonataxia symptoms. Neurology. 2008;71(13):982-9.

7. Kollmer J, Hund E, Hornung B, Hegenbart U, Schonland SO, Kimmich C, et al. In vivo detection of nerve injury in familial amyloid polyneuropathy by magnetic resonance neurography. Brain : a journal of neurology. 2015;138(Pt 3):549-62.
8. Kollmer J, Hilgenfeld T, Ziegler A, Saffari A, Sam G, Hayes JM, et al. Quantitative MR neurography biomarkers in 5q-linked spinal muscular atrophy. Neurology. 2019;93(7):e653-e64.
9. Pham M, Oikonomou D, Hornung B, Weiler M, Heiland S, Baumer P, et al. Magnetic resonance neurography detects diabetic neuropathy early and with Proximal Predominance. Ann Neurol. 2015;78(6):939-48.
10. Jende JME, Groener JB, Oikonomou D, Heiland S, Kopf S, Pham M, et al. Diabetic neuropathy differs between type 1 and type 2 diabetes: Insights from magnetic resonance neurography. Ann Neurol. 2018;83(3):588-98.
11. Schmitz-Hubsch T, du Montcel ST, Baliko L, Berciano J, Boesch S, Depondt C, et al. Scale for the assessment and rating of ataxia: development of a new clinical scale. Neurology. 2006;66(11):1717-20.
12. Jacobi H, Rakowicz M, Rola R, Fancellu R, Mariotti C, Charles P, et al. Inventory of Non-Ataxia Signs (INAS): validation of a new clinical assessment instrument. Cerebellum. 2013;12(3):418-28.
13. Tezenas du Montcel S, Durr A, Rakowicz M, Nanetti L, Charles P, Sulek A, et al. Prediction of the age at onset in spinocerebellar ataxia type 1, 2, 3 and 6. J Med Genet. 2014;51(7):479-86.
14. Rother C, Bumb JM, Weiler M, Brault A, Sam G, Hayes JM, et al. Characterization and quantification of alcohol-related polyneuropathy by magnetic resonance neurography. Eur J Neurol. 2022;29(2):573-82.
15. Kollmer J, Weiler M, Purrucker J, Heiland S, Schonland SO, Hund E, et al. MR neurography biomarkers to characterize peripheral neuropathy in AL amyloidosis. Neurology. 2018;91(7):e625-e34.
16. Kollmer J, Bendszus M. Magnetic Resonance Neurography: Improved Diagnosis of Peripheral Neuropathies. Neurotherapeutics. 2021;18(4):2368-83.
17. Heiland S, Sartor K, Martin E, Bardenheuer HJ, Plaschke K. In vivo monitoring of age-related changes in rat brain using quantitative diffusion magnetic resonance imaging and magnetic resonance relaxometry. Neuroscience letters. 2002;334(3):157-60.

18. Miot E, Hoffschir D, Alapetite C, Gaboriaud G, Pontvert D, Fetissof F, et al. Experimental MR study of cerebral radiation injury: quantitative T2 changes over time and histopathologic correlation. AJNR American journal of neuroradiology. 1995;16(1):79-85.
19. Walimuni IS, Hasan KM. Atlas-based investigation of human brain tissue microstructural spatial heterogeneity and interplay between transverse relaxation time and radial diffusivity. NeuroImage. 2011;57(4):1402-10.
20. Kollmer J, Sahm F, Hegenbart U, Purrucker JC, Kimmich C, Schonland SO, et al. Sural nerve injury in familial amyloid polyneuropathy: MR neurography vs clinicopathologic tools. Neurology. 2017;89(5):475-84.
21. Jende JME, Hauck GH, Diem R, Weiler M, Heiland S, Wildemann B, et al. Peripheral nerve involvement in multiple sclerosis: Demonstration by magnetic resonance neurography. Ann Neurol. 2017;82(5):676-85.
22. Rother C, Bumb JM, Weiler M, Brault A, Sam G, Hayes JM, et al. Characterization and quantification of alcohol-related polyneuropathy by magnetic resonance neurography. Eur J Neurol. 2021.
23. Berciano J, Infante J, Garcia A, de Pablos C, Amer G, Polo JM, et al. Stiff man-like syndrome and generalized myokymia in spinocerebellar ataxia type 3. Mov Disord. 2006;21(7):1031-5.
24. Schols L, Linnemann C, Globas C. Electrophysiology in spinocerebellar ataxias: spread of disease and characteristic findings. Cerebellum. 2008;7(2):198-203.
25. Nijeholt GJ, Bergers E, Kamphorst W, Bot J, Nicolay K, Castelijns JA, et al. Post-mortem high-resolution MRI of the spinal cord in multiple sclerosis: a correlative study with conventional MRI, histopathology and clinical phenotype. Brain : a journal of neurology. 2001;124(Pt 1):154-66.
26. Does MD, Beaulieu C, Allen PS, Snyder RE. Multi-component T1 relaxation and magnetisation transfer in peripheral nerve. Magn Reson Imaging. 1998;16(9):1033-41.
27. Kollmer J, Kastel T, Jende JME, Bendszus M, Heiland S. Magnetization Transfer Ratio in Peripheral Nerve Tissue: Does It Depend on Age or Location? Invest Radiol. 2018;53(7):397-402.
28. Wolff SD, Balaban RS. Magnetization transfer contrast (MTC) and tissue water proton relaxation in vivo. Magn Reson Med. 1989;10(1):135-44.

29. McGowan JC. The physical basis of magnetization transfer imaging. Neurology. 1999;53(5 Suppl 3):S3-7.
30. Dortch RD, Dethrage LM, Gore JC, Smith SA, Li J. Proximal nerve magnetization transfer MRI relates to disability in Charcot-Marie-Tooth diseases. Neurology. 2014;83(17):1545-53.
31. Kollmer J, Hegenbart U, Kimmich C, Hund E, Purrucker JC, Hayes JM, et al. Magnetization transfer ratio quantifies polyneuropathy in hereditary transthyretin amyloidosis. Ann Clin Transl Neurol. 2020;7(5):799-807.
32. Kollmer J, Kessler T, Sam G, Hayes JM, Lentz SI, Heiland S, et al. Magnetization transfer ratio: a quantitative imaging biomarker for 5q spinal muscular atrophy. Eur J Neurol. 2021;28(1):331-40.

Figure legends

Figure 1.

Quantitative MRN markers

Nerve ρ (A), $T2_{app}$ (B), MTR (C), and CSA (D) mean values at thigh level were plotted separately for each group in a box and whisker plot. All quantitative markers differentiated well between healthy controls and all SCA3 mutation carriers by a significant decrease. In addition, ρ, MTR, and CSA separated SCA3 mutation carriers without electrophysiologically manifest PNP as well as pre-ataxic SCA3 mutation carriers from controls, while $T2_{app}$ only identified SCA3 patients with manifest PNP. Further differentiation between SCA3 mutation carriers with and without PNP was only possible by analyzing sciatic nerve MTR.

ρ = proton spin density; $T2_{app}$ = apparent T2-relaxation time; MTR = magnetization transfer ratio; CSA = cross-sectional area. SCA3 = SCA3 mutation carrier; SCA3 PNP+ = SCA3 mutation carriers with polyneuropathy; SCA3 PNP- = SCA3 mutation carriers without polyneuropathy. Significant differences are indicated by either * = significant ($p \leq 0.05$), or *** = highly significant ($p \leq 0.001$).

Figure 2.

MRN source images

Representative magnetic resonance neurography (MRN) images (axial dual-echo turbo spin echo relaxometry sequences with spectral fat saturation) at left midthigh level are shown at equal slice positions in a healthy control (A), a SCA3 mutation carrier without PNP (B), and a SCA3 mutation carrier with PNP (C). Details show the tibial and peroneal fascicles within the sciatic nerve. Note the slight decrease in sciatic nerve T2w signal, a consequence of the decrease in both, ρ and $T2_{app}$, and sciatic nerve CSA in SCA3 PNP- (B), and in SCA3 PNP+ (C) compared to the healthy control (A). * indicates perineural vessels.

Figure 3.

Magnetization transfer ratio map

Representative MTR pseudo-colorized (%) maps are shown for a healthy control (A), a SCA3 mutation carrier without PNP (B), and a SCA3 mutation carrier with PNP (C). The white boxes in A-C are zoomed-in and displayed below to show detailed views of the MTR (%) map (left) and the MTC sequence without the off-resonance pulse (right) with the sciatic nerve at the left mid-thigh encircled in white. Note the marked decrease of sciatic nerve MTR (%) in SCA PNP- (B; loss of red and yellow signals), and even further decrease in SCA3 PNP+ (C) compared to the healthy control (A).

Table legend

Table 1.

Demographic, clinical and electrophysiologic data

SCA3 = SCA3 mutation carrier; SCA3 PNP+ = SCA3 mutation carriers with polyneuropathy; SCA3 PNP- = SCA3 mutation carriers without polyneuropathy. SARA = scale of the assessment and rating of ataxia; INAS = inventory of non-ataxia signs; PTR = patellar tendon reflex; ATR = Achilles tendon reflex; disease stage 0 = no gait problems, 1 = ataxic, do not need a walking aid, 2 = permanently using a walking aid, 3 = wheelchair bound; Pallhypesthesia: none = 8/8, mild = >5/8, moderate = 2-5/8, severe = < 2/8; SNAP = sensory nerve action potential; RSN = right sural nerve; LSN = left sural nerve; CMAP = compound muscle action potential; RPN = right peroneal nerve; LTN = left tibial nerve; DML = distal motor latency; NCV = nerve conduction velocity.

All results are presented as mean values +/- standard error of the mean.

ns = not significant, * = significant ($p \leq 0.05$), *** = highly significant ($p \leq 0.001$)

Table 1: Demographic, clinical and electrophysiologic data

Parameter	SCA3 (n = 18)	SCA3 PNP+ (n = 6)	SCA3 PNP- (n= 12)	p value SCA3-PNP+ vs. SCA3 PNP-
Age (years)	42.3 ± 3.0	54.7 ± 2.7	36.1 ± 2.9	0.0069*
Sex (m/f)	9 / 9	4 / 2	5 / 7	n.a.
Body weight (kg)	74.2 ± 2.8	80.0 ± 2.3	71.3 ± 3.8	0.20 (ns)
Height (cm)	1.75 ± 0.02	1.76 ± 0.05	1.75 ± 0.03	0.57 (ns)
Body mass index (kg/m²)	24.2 ± 0.8	26.1 ± 1.5	23.2 ± 0.9	0.35 (ns)
CAG long allele	68.7 ± 0.9	67.5 ± 0.4	69.3 ± 1.4	0.29 (ns)
CAG short allele	25.3 ± 3.1	28.4 ± 8.1	23.4 ± 1.6	0.65 (ns)
SARA (0-40 points)	7.86 ± 1.72	15.25 ± 2.89	4.17 ± 1.09	0.0005***
INAS (0-16 points)	2.83 ± 0.51	5.33 ± 0.67	1.58 ± 0.29	<0.0001***
PTR areflexia / normal / hyperreflexia	4 / 12 / 2	3 / 3 / 0	1 / 9 / 2	n.a.
ATR areflexia / normal / hyperreflexia	7 / 9 / 2	5 / 1 / 0	2 / 8 / 2	n.a.
Pallhypesthesia (none / mild / moderate / severe)	3 / 9 / 4 / 2	0 / 0 / 4 / 2	3 / 9 / 0 / 0	n.a.
Disease stage (0 / 1 / 2 / 3)	7 / 9 / 1 / 1	0 / 4 / 1 / 1	7 / 5 / 0 / 0	n.a.
SNAP (µV)				
RSN	10.1 ± 1.6	3.4 ± 0.9	12.9 ± 1.6	0.0005***
LSN	8.4 ± 1.5	3.0 ± 0.7	10.9 ± 1.7	0.0009***
CMAP (mV)				
RPN	5.9 ± 0.8	3.3 ± 1.2	7.2 ± 0.9	0.0105*

LTN	17.4 ± 2.1	9.2 ± 2.7	21.6 ± 2.1	0.0065*
DML (ms)				
RPN	4.4 ± 0.2	5.0 ± 0.6	4.1 ± 0.2	0.10 (ns)
LTN	3.8 ± 0.1	3.7 ± 0.1	3.8 ± 0.1	0.84 (ns)
NCV (m/s)				
RPN	45.9 ± 1.1	42.2 ± 1.9	47.8 ± 1.1	0.0163*
LTN	47.3 ± 0.8	45.5 ± 1.4	48.1 ± 1.0	0.11 (ns)
RSN	49.4 ± 1.2	46.8 ± 2.5	50.5 ± 1.2	0.22 (ns)
LSN	48.2 ± 1.4	45.0 ± 2.1	49.6 ± 1.6	0.10 (ns)

SCA3 = SCA3 mutation carrier; SCA3 PNP+ = SCA3 mutation carriers with polyneuropathy; SCA3 PNP- = SCA3 mutation carriers without polyneuropathy. SARA = scale of the assessment and rating of ataxia; INAS = inventory of non-ataxia signs; PTR = patellar tendon reflex; ATR = Achilles tendon reflex; disease stage 0 = no gait problems, 1 = ataxic, do not need a walking aid, 2 = permanently using a walking aid, 3 = wheelchair bound; Pallhypesthesia: none = 8/8, mild = >5/8, moderate = 2-5/8, severe = < 2/8; SNAP = sensory nerve action potential; RSN = right sural nerve; LSN = left sural nerve; CMAP = compound muscle action potential; RPN = right peroneal nerve; LTN = left tibial nerve; DML = distal motor latency; NCV = nerve conduction velocity.

All results are presented as mean values +/- standard error of the mean.

ns = not significant, * = significant ($p \leq 0.05$), *** = highly significant ($p \leq 0.001$)

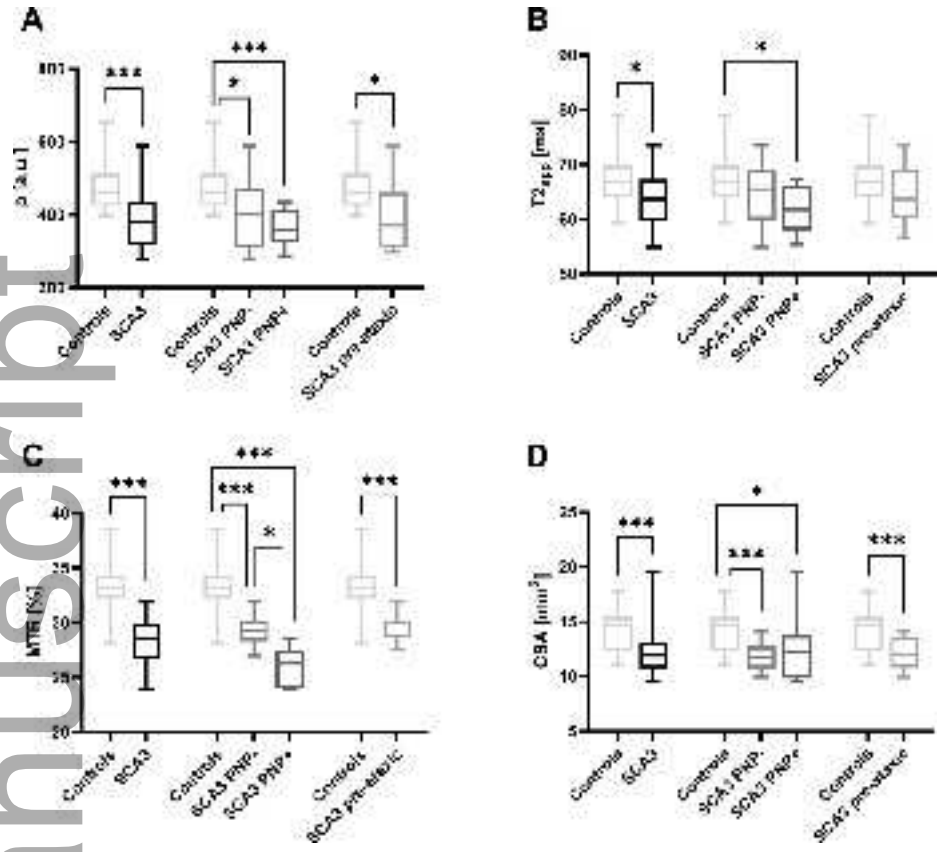

ene_15305_f1.tif

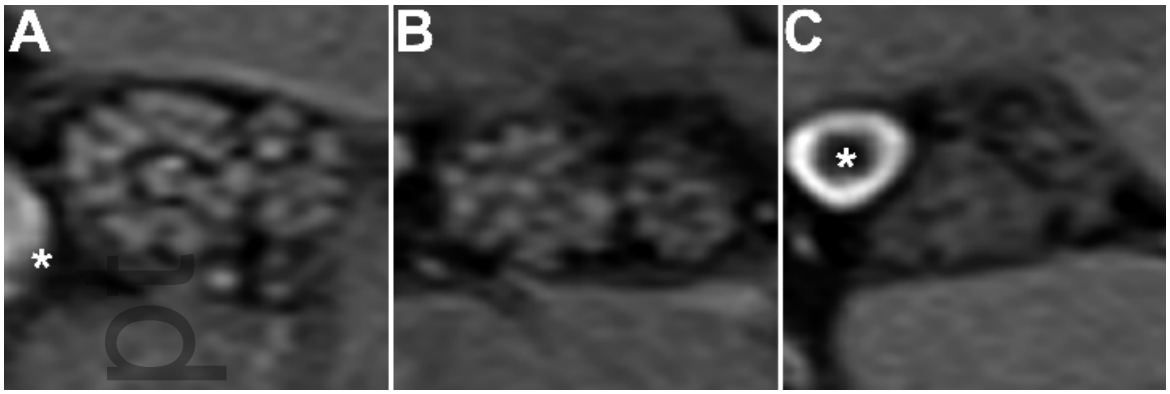

ene_15305_f2.tif

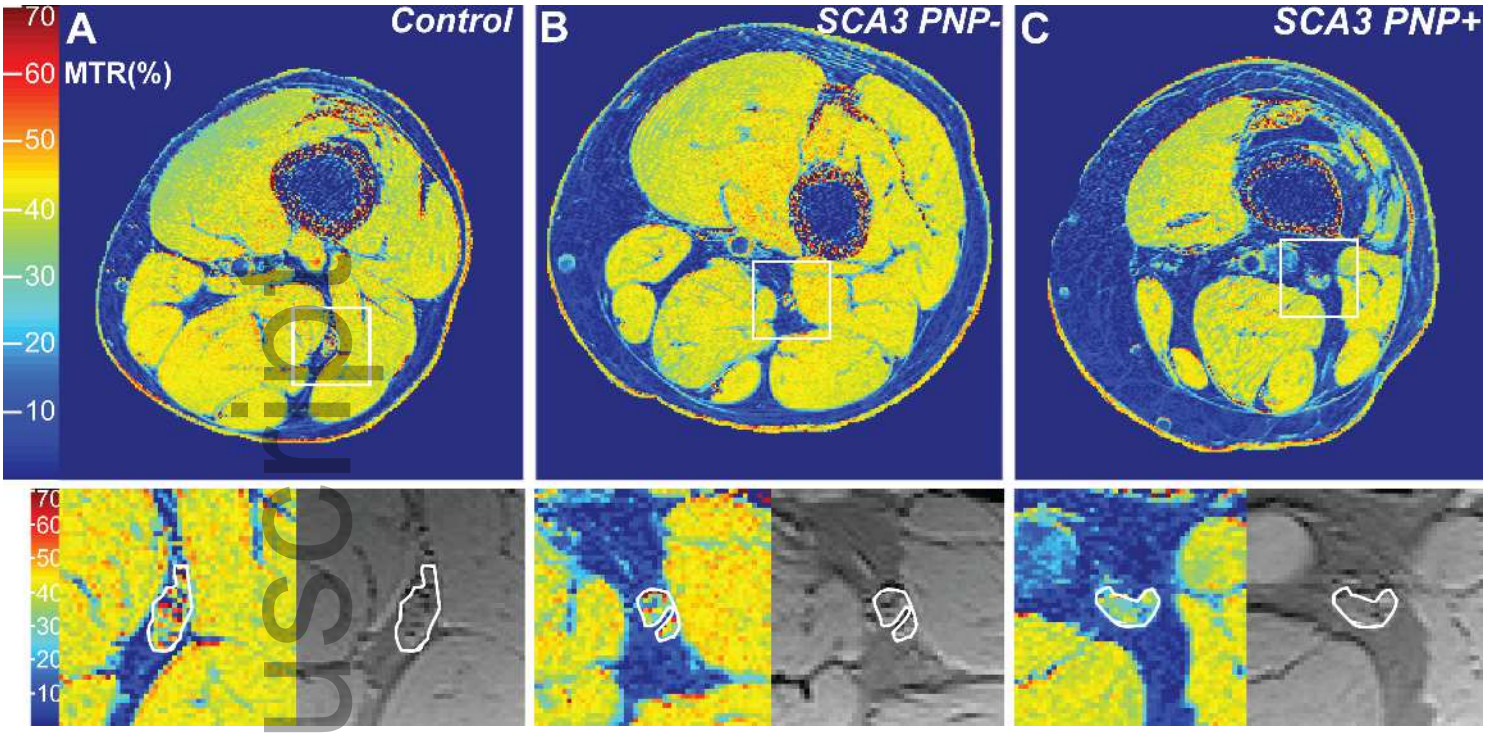

ene_15305_f3.tif